On a Tollmien–Schlichting wave packet produced by a turbulent spot

By I. WYGNANSKI,† J. H. HARITONIDIS
AND R. E. KAPLAN

University of Southern California, Los Angeles

Experimental investigations in the region following the passage of an isolated turbulent spot in a laminar boundary layer reveal the existence of a pair of oblique wave packets. These packets are swept at an angle of approximately 40°, and exhibit frequency and wave speed characteristics in agreement with predictions made for oblique Tollmien–Schlichting waves. No waves exist near the centreline of the spot.

Several observations of the breakdown of this ordered motion into a new turbulent spot are shown. This breakdown is accompanied by the appearance of an intense shear layer inclined to the wall.

1. Introduction

The turbulent spot, first observed in shallow water flow by Emmons (1951), was investigated extensively by Schubauer & Klebanoff (1956) who established its role in the transition process. Recently, the spot was investigated by Komoda (1974), Coles & Barker (1975), Wygnanski, Sokolov & Friedman (1976) and Cantwell, Coles & Dimotakis (1977). Wygnanski *et al.* (1976) charted the shape of the spot in three dimensions and established that far downstream it becomes independent of the initial disturbance. They also provided the mean velocity field within the spot. Cantwell *et al.* (1977) calculated the mean particle trajectories relative to the spot and proposed that the sublayer streaks, which were observed in the spot using flow visualization techniques, are caused by a Taylor–Görtler type of instability.

This renewed interest in the turbulent spot stems partly from interest in boundary-layer transition, as well as from observations pertaining to the existence of large coherent eddies in the turbulent boundary layer. Since the final transition to turbulence in a boundary layer is accomplished by the amalgamation of such spots, the possibility exists that the spot and the 'large eddy' may have some common properties. This notion was explored by Zilberman, Wygnanski & Kaplan (1976) who showed that a portion of the spot survived the random buffeting by the surrounding turbulence in a turbulent boundary layer over extraordinarily long distances. The structure thus observed exhibits features which agree in detail with those in the outer bulges of a turbulent boundary layer (Kovasznay, Kibens & Blackwelder 1970). The structure is 2δ to 4δ long (in the streamwise direction) in the region of the interface and extends

† Present address: School of Engineering, Tel Aviv University, Ramat Aviv, Tel Aviv, Israel.

to approximately 10δ closer to the surface. In the spanwise direction, it measures approximately 1–3δ, although this figure is maybe an upper bound on its extent. Since the spacing between sublayer streaks ($z^+ = Uz/\nu \simeq 100$) is of the order of 0.1–0.2δ in typical experiments, there is an order of magnitude difference between the width of the outer bulge and the sublayer streak in the turbulent boundary layer. If the difference is real, then there must exist a mechanism which is reponsible for the additional fragmentation of the large eddy in the spanwise direction. Cantwell *et al.* (1977) attribute the fragmentation to an instability of the Taylor–Görtler type which must be associated with a local curvature of flow. It is suggested that such an instability exists under the nose overhang of the spot's leading interface. Furthermore, one would expect to find weak, but fairly regular streamwise vorticity in the 'calmed' region which follows the spot. Flow visualization methods using dye and aluminium particles are brought as evidence for this mechanism of instability.

Klebanoff, Tidstrom & Sargent (1962) attribute the generation of small scale turbulence to the breakdown of Tollmien–Schlichting waves, which they explain by preferential amplification in the spanwise direction resulting from undetectably small fixed irregularities in the apparatus. The resultant concentration of vorticity in a narrow region gives rise to a local inflexional velocity profile which is highly unstable and would generate eddies having a scale proportional to the width of the local shear-layer (see figures 30 and 31 of Klebanoff *et al.* 1962). This scale is approximately equal to 0.2δ, which is comparable with the scale of the boundary-layer streaks.

It is the purpose of the present study to explore a mechanism which could contribute to the generation of smaller scales, as well as investigate the existence of possible regeneration processes of a turbulent spot. The puffs in transitional pipe-flow observed by Wygnanski, Sokolov & Friedman (1975) tend to split with increasing Reynolds number, yet there is no evidence for such splitting of a turbulent spot. Indeed, some kind of regeneration process is necessary to make the correlation between the spot and the large coherent eddy more plausible.

2. Experimental equipment

The wind tunnel used in these experiments is almost identical to the one reported by Wygnanski *et al.* (1976), the major difference being that the tunnel circuit is located in a vertical plane. The test section is 2 ft wide, 3 ft high and 20 ft long. All measurements were made on the working side of a 'flat plate' located vertically in the test section and at a nominal distance of 7 in. from one of the vertical walls, thus dividing the test section into a wide (primary) and a narrow (secondary) channel. It consists of a 0.25 in. thick, 11.5 ft long aluminium plate followed by a 0.5 in. thick, 7.5 ft long Plexiglas plate. The aluminium plate has a rounded leading edge and is polished to a mirror-like finish.

The width of the primary channel increases with downstream distance in order to maintain a nominally zero pressure gradient. A metal screen was placed at the end of the primary channel having a pressure drop approximately equal to the total pressure drop along the secondary channel. An adjustable flap attached to the end of the Plexiglas plate allowed accurate positioning of the stagnation streamline at the leading edge of the 'flat plate'. Measurements of the static pressure distribution along the primary channel showed dc_p/dx to be no greater than -0.001 in.$^{-1}$ for the velocities

of interest, where $c_p = 2p/\rho U_\infty^2$. The streamwise component of the turbulence level was approximately 0·04 %.

Constant temperature hot-wire anemometers, operated at a resistance overheat of 30 %, were used throughout this investigation. The wire material was 10 % Rh-Pt, 0·0001 in. in diameter and was always soft-soldered to the probe prongs. The frequency response, as determined by the square wave technique, was better than 10 kHz.

The probes employed were either single or multiple (rake) wire probes. The single wire probes consist of jeweller's broaches 0·4 in. long and 0·045 in. apart, protruding from a ceramic stem 0·057 in. in diameter. The diameter of the broaches near the stem is 0·005 in. and they taper to 0·002 in. at the tips. Two y rakes (normal to the plate) and one z rake (parallel to the plate and transverse to the flow) were used to measure the instantaneous streamwise velocity.

The z rake was the same as the one used by Blackwelder & Kaplan (1976). It has 12 wires 0·030 in. long with a centre to centre separation of 0·100 in. In the present experiments, the wire lengths were reduced to 0·020 in. The two y rakes are identical in construction and differ only in the wire separation. 10 pairs of jeweller's broaches, similar to the ones used for the single probes, were epoxied onto a 0·5 in. wide, 2 in. long and 0·055 in. thick slab of epoxy–fibreglass circuit board material. The broaches extend 0·4 in. ahead of the rounded leading edge of the slab and have a tip separation of 0·044 in. The wire distances (in thousandths of an inch) from the bottom of the corresponding rakes are: (20, 40, 60, 80, 100, 120, 150, 200, 250, 300) and (40, 80, 120, 160, 240, 320, 440, 600, 760, 1000). Microdot (TM) connectors were epoxied to the top of each slab serving the dual purpose of electrical and structural connectors to the probe holder (figure 1, plate 1).

The probe-traversing mechanism could be positioned manually anywhere along the length of the plate. Electric motors controlled the y and z positions with a respective accuracy of $\pm\,0{\cdot}0005$ in. and $\pm\,0{\cdot}010$ in.

3. Data acquisition and reduction

The data reduction and stability calculations were made on a PDP11/55 mini-computer, using FORTRAN programs. Each analog input channel was provided with its own integral sample and hold amplifier to acquire the data on all channels simultaneously under program control. The initial experiment was performed several months before the arrival of the computer so all calibration and measurements were recorded on 14 channel FM analog tape. One channel contained a basic timing signal which controlled the automotive electronic ignition used to generate the turbulent spot. The input of this channel was connected to a comparator which drove a TTL digital input of the computer. The trailing edge of this control pulse was sensed with a 500 μs resolution, then a preprogrammed delay (in the range 50–100 ms) lapsed before sampling commenced. Samples were taken for a duration sufficient to bracket the data, and in general the sampling interval was on the order of 150 ms. After the initial results were processed, certain measurements were repeated and the analog tape was not used since the data could be acquired by the computer in 'real time'. The entire digitized record was buffered in computer memory and written to digital tape in one block with an identification prefix. These digital tapes then became the

primary experimental record. Graphical output was *via* one of the terminals connected to the computer, which gave a quick 'numberless' check on results.

The calculations of the eigenvalues of the Orr–Sommerfeld equation were performed on the same computer. The programs were originally written for an IBM 709 computer (Kaplan 1964), modified for a Honeywell 800 (Landahl & Kaplan 1965) and subsequently modified for operation on an IBM 360/44 computer and the DECSYSTEM 10 (1080T). The velocity profiles were specified as tables to only 5 significant figures (IBM 360 limitation) and limit the accuracy of the results. Eigenvalues were computed as described by Kaplan (1964) and, whereas accuracy of 4 significant figures was specified, generally are accurate to at least 5 significant figures for complex phase speed (subject to the limitations of the accuracy of the tabulated velocity profiles).

4. Results

4.1. *On the wave packet trailing the turbulent spot*

In the exploratory stages of the experiment the flow field downstream of the spark was traversed with hot wires whose output was monitored on an oscilloscope. When the turbulent region directly downstream of the spark (i.e. in the central zone of the spot) did not reveal the existence of spatially coherent structures, the investigation focused on the laminar flow surrounding the spot. It was hoped that large, coherent structures in the turbulent region will induce clearly observable potential fluctuations as they do in the two-dimensional mixing region (Oster, Wygnanski & Fiedler 1976). However, preliminary observations in the vicinity of the plane of symmetry, did not reveal any fluctuations of this type, not even in the calmed region where flow visualization methods (Elder 1962; Cantwell *et al.* 1977) indicate the existence of orderly streamwise vortices. The observations of Mochizuki (1961) on the transition behind a spherical roughness element suggested that a pair of vortices may trail the tips of the spot in a way which is analogous to wing-tip vortices. It was in this vicinity that a wave packet trailing the spot was first observed.

An example of the simultaneous streamwise velocity signals as a function of the spanwise z co-ordinate is shown in figure 2. The data shown were obtained at

$$Re_x = Ux/\nu = 1{\cdot}59 \times 10^6$$

and $y/\delta = 0{\cdot}2$, where x is the distance from the leading edge of the plate, and δ is the laminar boundary-layer thickness. The distance from the spark $x_s = 2$ ft and the spark was located 1 ft from the leading edge ($x_{sp} = 1$ ft). Note that the time scale (which forms a streamwise dimension using a characteristic convection velocity of the spot) is highly compressed in comparison to the spanwise dimension (Δz between adjacent wires $= 0{\cdot}1$ in.). The wave packet appears behind the spot (i.e. it arrives at the measuring station at a later time), it is inclined to the time axis and extends (in the z direction) beyond the physical boundaries of the spot. Two independent hot-wire probes were used to observe individual realizations and establish approximately the gross behaviour of the wave packet. Although the following data were obtained at $x_{sp} = 1$ ft, $x_s = 2$ ft and $U_\infty = 35$ ft/s, the results are fairly general.

(1) The crest velocity of the waves in the packet in the direction of streaming (see appendix) was determined locally by placing the second hot wire directly downstream of the first one at the same distance from the wall. The output of two such wires is
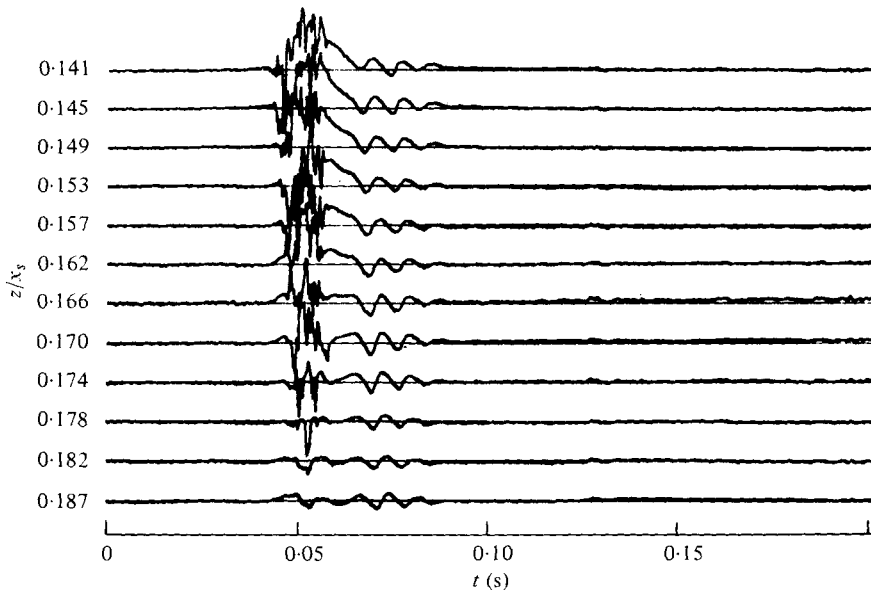
FIGURE 2. Example of spot and trailing wave packet. $Re_x = 1.59 \times 10^6$, $y/\delta = 0.2$, $z/x_s = 0.141$–0.187.

shown in figure 3 (a) (plate 2) where the distance between the wires was 0.75 in. The phase lag between the output of these wires is clearly visible and averaged over a number of realizations yielded a crest velocity c_{cr} to be approximately 40 % of the free stream velocity. This should be compared to the speed at which the trailing edge of the spot is convected, i.e. approximately one half of the free stream speed.†

(2) The inclination ψ of the wave packet to the plane of symmetry was first estimated from records similar to figure 2 to be approximately 45°. The estimate was checked by using two wires which were displaced in both the streamwise and spanwise directions. The displacement Δx was adjusted until the output of both wires was precisely in phase. In the example shown in figure 3 (b) the wires were spaced by $\Delta z = 0.45$ in., $\Delta x = 0.49$ in., giving an angle $\psi \sim 47°$.

(3) The wave packet appears to ride on the Blasius profile. As we look closer to the trailing edge of the spot (at a given z) the wave disappears as the flow accelerates to match the wall shearing stress in the spot. The wave packet is not visible in the 'calmed region' near the plane of symmetry of the spot. In figure 3 (c) two velocity traces taken simultaneously are shown. The upper trace is from a hot wire which is located on the plane of symmetry while the lower trace was taken 5 in. off the plane of symmetry. In the former case no wave packet can be seen.

† At the early stages of the experiment higher crest speeds were seemingly observed as a result of probe interference. The measurements were repeated to determine the crest speed more accurately using three wires in a non-interfering geometric arrangement to obtain c_{cr}, ψ and f simultaneously. The signal from each wire was digitally Fourier analysed during the specified time window. Differences in the phase of two independent pairs of wires were used to solve for both components of the wave number vector at selected frequencies. Averages of wave number amplitude and angle could then be computed (or, alternatively, average phase speed and angle). The best fit frequency for the packet was selected from the narrowest histogram of a 200 sample set, and always corresponded to the spectral peak of the waves.
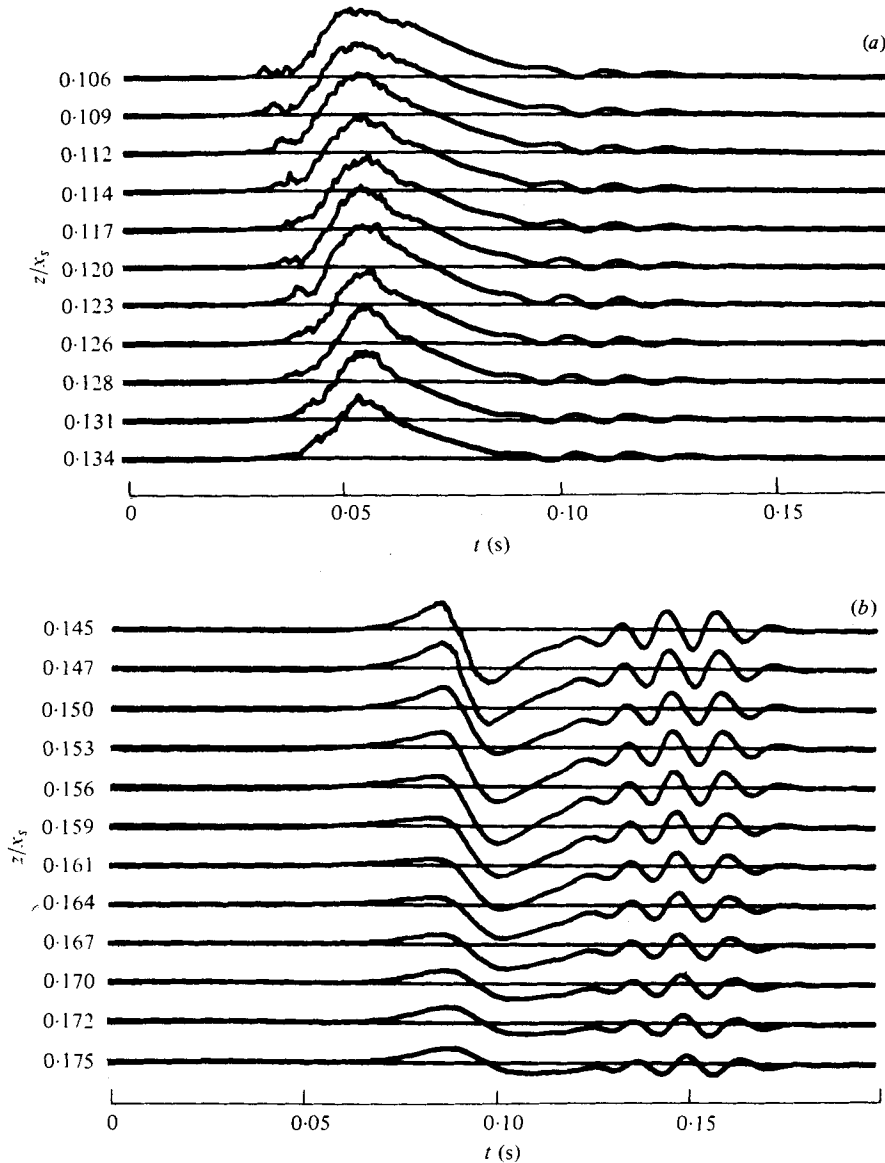
FIGURE 4. Ensemble average of 100 events. $x_{sp} = 1$ ft, $x_s = 3$ ft,
$U_\infty = 35$ ft/s. (a) $z/x_s = 0\cdot106$–$0\cdot134$. (b) $z/x_s = 0\cdot145$–$0\cdot175$.

(4) The number of waves in the packet increases with increasing distance from the
spark. The wave packet appeared so regularly that an ensemble average of many
events was attempted. The ensemble was generated in the most simple way, i.e. by
triggering the instrumentation on the electric pulse accompanying the spark. It
became evident that the time of arrival of the wave packet is more precisely repeat-
able than the time of arrival of the spot (i.e. either the leading or trailing interface).

Two examples of such an ensemble containing 100 events are shown in figure 4 (a, b).
The edges of the turbulent region can be deduced from the slightly rugged appearance
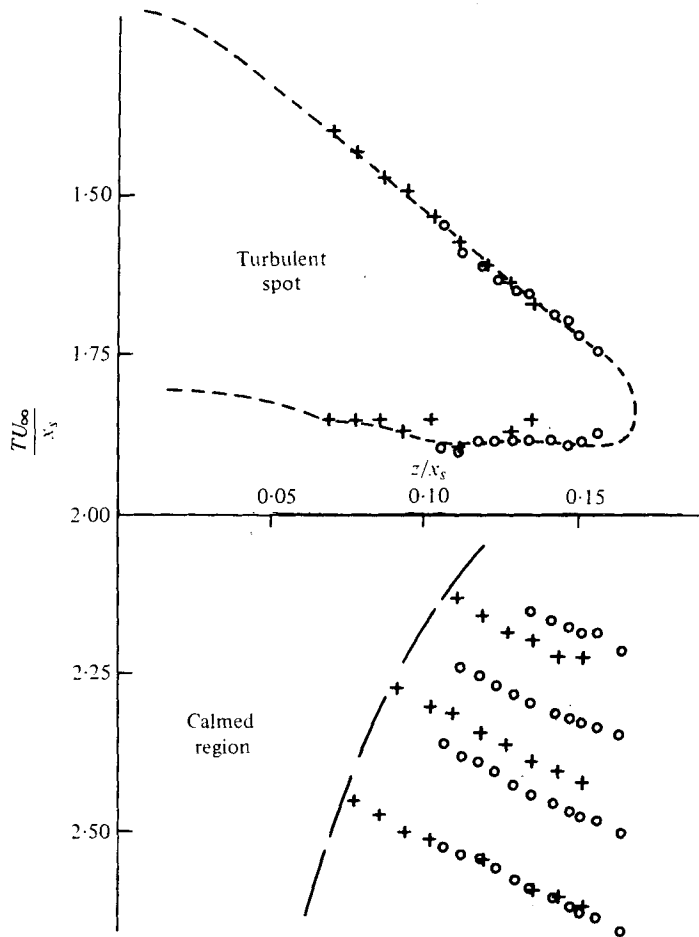
FIGURE 5. Geometric relationship of wave packet to spot. $U_\infty = 35$ ft/s, $x_{s\rho} = 1$ ft. $+$, $x_s = 2$ ft; $\bigcirc$, $x_s = 3$ ft.

of the velocity since the turbulent fluctuations did not average out entirely because of the relatively small number of events in the ensemble. Following the spot (figure 4a) there is a slow deceleration to the prevailing undisturbed velocity, and only then does the wave packet appear. Beyond the turbulent region the situation reverses and the flow accelerates towards the wave packet (figure 4b). The frequency of the waves in the packet can be determined with fair accuracy directly from such figures although spectral analysis was used to confirm the observations. The inclination of the waves to the plane of symmetry can also be obtained from figure 4(a) by using the approximate crest speed; however two-point space–time correlations were taken in order to verify the results. The benefits of statistical techniques can only be realized at higher Reynolds numbers when nonlinearities appear in the wave packet.

The geometrical relationship between the spot and the wave packet is shown in figure 5. The abscissa and ordinate in this figure were rendered dimensionless through division by x_s, which is the similarity parameter for the spot. The appropriate boundaries of the spot collapse on one curve although two sets of measurements, 2 and 3 feet
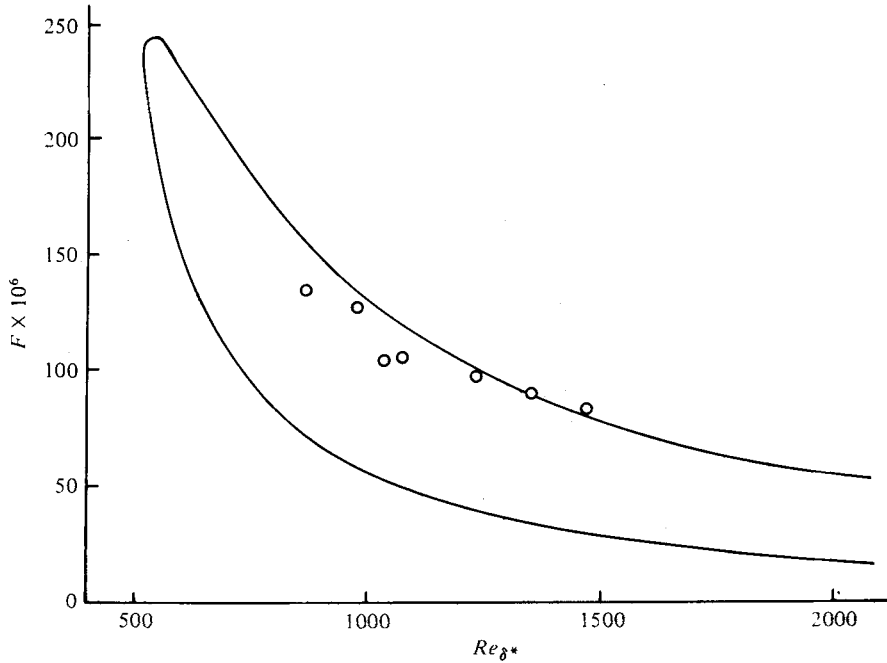
FIGURE 6. Non-dimensional frequency $F = 2\pi f \nu / U_\infty^2$ vs. Re_{δ^*}.

downstream of the spark, are presented. The visible troughs of the waves in the packet are also shown. The location of the wave packets relative to the spot seems to scale in the same way as the spot boundaries although the constant phase lines of the two tests do not collapse onto one another. The entire group of waves lags behind the spot trailing edge, and the distance between the two increases with x. There is also a Reynolds number effect since the frequency of the waves in the packet decreases with increasing Re. All of these observations are consistent with a wave packet moving slightly slower than the spot, with the speed of the packet slightly greater than 40 % of free stream speed. The disappearance of the waves close to the plane of symmetry corresponds to the observations of a 'calmed' region behind the spot.

4.2. *Comparison with linear stability calculations*

Table 1 summarizes the experimental data base.

Assuming that the waves are superimposed on the Blasius profile, the results of the linear stability theory, for two-dimensional waves, can be easily applied using Squire's transformation if the angle ψ between the wavenumber vector of the oblique waves and the streamwise direction is known. The Reynolds number should be multiplied by $\cos \psi$ and the dimensionless frequency F divided by $\cos \psi$ (see appendix). All points fall near branch II of the neutral stability curve which represents the condition for maximum total amplification appropriate to the local Reynolds number at which the measurements were taken (figure 6). The frequency of the waves in the packet decreases as it propagates downstream (table 1), thus adjusting continuously to this condition. These observations differ from the vibrating ribbon experiments (Schubauer & Skramstad 1948) in which the frequency was constant. The results at $Re_{\delta^*} > 1800$

Case ...	1	2	3	4	5	6	7
U_∞ (ft/s)	25	35	50	59	25	35	50
z (in.)	-3	-3	-3	-3_1	$-4\cdot5$	$-4\cdot5$	$-4\cdot5$
x_{sp} (ft)	1	1	1	1	1	1	1
x_s (ft)	2	2	2	2	3	3	3
x (ft)	3	3	3	3	4	4	4
Re_{δ^*}	1050	1240	1640	1900	1210	1430	1890
f (Hz)	53	85	131	165	50	70	111
$F \times 10^{-6}$	88	72	55	49	83	59	46
ψ°	36	33	41	39	36	41	44
$Re_{\delta^*} \cos \psi$	870	1040	1240	1480	980	1080	1360
$F/\cos^2 \psi \times 10^6$	134	103	96	82	127	104	89
c_{cr}/U_∞	0·35	0·33	0·30	0·30	0·33	0·29	0·35
c/U_∞	0·37	0·36	0·36	0·35	0·37	0·36	0·36

TABLE 1. Representative characteristics of the wave packet: z = spanwise position measured from the centreline of the plate. $x = x_{sp} + x_s$, distance from the leading edge of the plate. δ^* = displacement thickness determined by direct measurement. $Re = U_\infty \delta^*/\nu$. $F = 2\pi f \nu/U_\infty^2$, where f is the dominant frequency of the wave packet. c_{cr} = crest speed of the waves. c = wave speed obtained through Squire's transformation.

are not very reliable because nonlinear effects were observed in many realizations and even a partial breakdown was noticed at the higher Reynolds numbers. The last two rows in table 1 should be the same for perfect agreement between theory and experiment (see appendix). However the discrepancies can be attributed in part to the fact that the aspect ratio of the waves, i.e. the ratio of their length to their wavelength, is about 3 at most, rather than infinite. Furthermore, the boundary layer behind the spot is three-dimensional.

The two components of the group velocity in the streamwise and spanwise directions were calculated as outlined in Gaster (1968), for the waves in the packets of figure 5. Their centroid is convected at $0\cdot42U_\infty$ in the streamwise direction and spreading at an angle of $7\cdot5°$. These numbers are in good agreement with the computed values of $0\cdot38U_\infty$ and $8°$ respectively.

The simultaneous streamwise velocities obtained with the small y rake (which contains 10 hot wires displaced in the direction normal to the surface of the plate) provide information about the character of the wave packet in this direction. Once again the individual realizations were sufficiently repeatable to warrant the formation of simple ensemble averages which are conditioned to the spark. Seven ensemble-averaged velocity records collected at the very edge of the spot ($z/x_s = 0\cdot156$) three feet downstream of the spark are shown in figure 7(a). The signature of the spot is marked by a long-wave velocity defect except at $y/\delta = 0\cdot083$, where some excess velocity was observed. The wave packet contains three easily distinguishable waves which are not in phase in the y direction (figure 7b). The maximum amplitude of the wave packet occurs at $y/\delta < 0\cdot25$ which is predicted by the linear stability theory. The peak-to-peak amplitude of the central wave at $y/\delta = 0\cdot25$ is approximately equal to $3\cdot4 \% U$ (or $1\cdot5 \% U_\infty$).

A quantitative measure of the amplitude distribution of the wave packet in the direction normal to the surface is obtained from power spectra. Ideally, one would
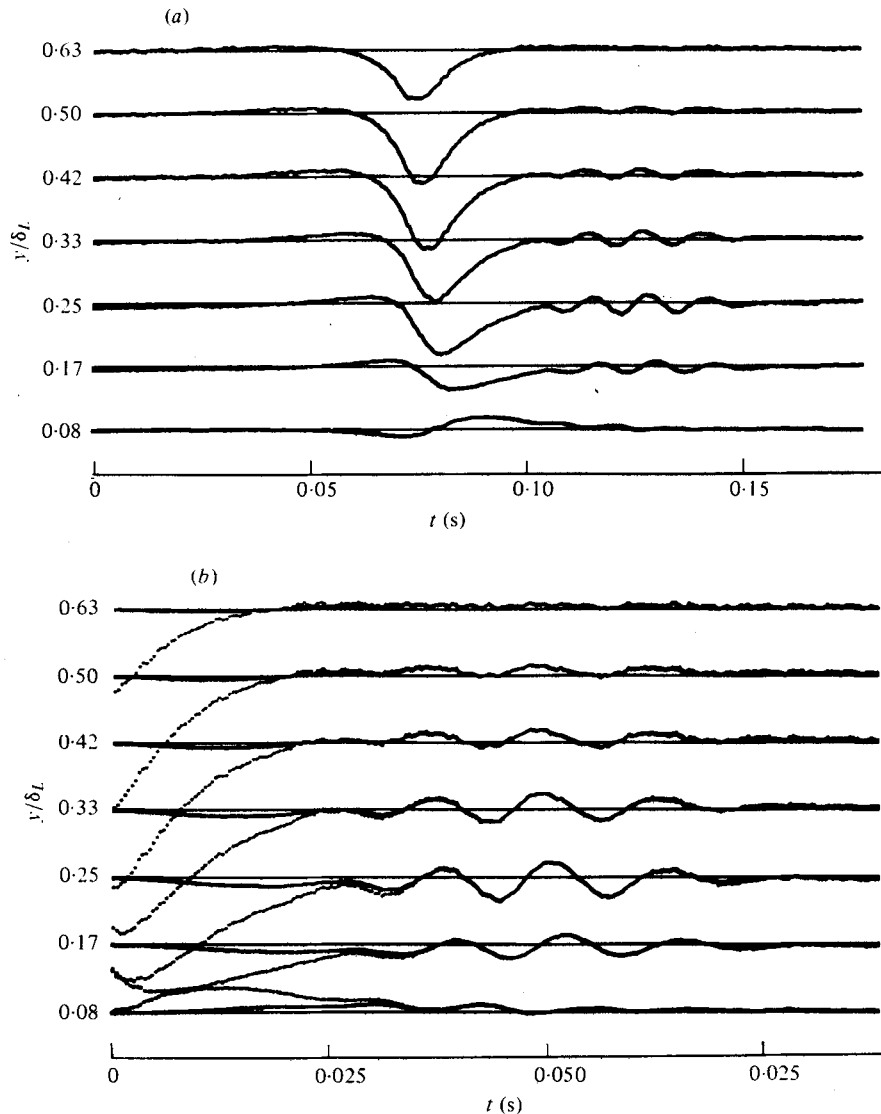
FIGURE 7. Ensemble average of 7 events. $x_{sp} = 1\,\text{ft}$, $x_s = 3\,\text{ft}$, $U_\infty = 35\,\text{ft/s}$, $z/x_s = 0\cdot156$. (a) No filtering. (b) With filtering.

like to disregard the low frequency accompanying the spot passage and measure the spectra of the wave packet only. This is done by applying Hanning weights to the transformed data and ensuring that the wave packet is centred in the Hanning window. The dotted lines in figure 7(b) represent part of the original data shown in figure 7(a) (both time and velocity scales are double in figure 7b). The solid lines represent reconstituted data which was Fourier analysed, Hanned and retransformed for comparison purposes. The two lines match perfectly in the central region of the figure, but the low frequencies associated with the passage of the spot are almost entirely eliminated. Since the power-spectra obtained in this way are quite well defined, *it is assumed* that the peak in the spectrum is proportional to u'.
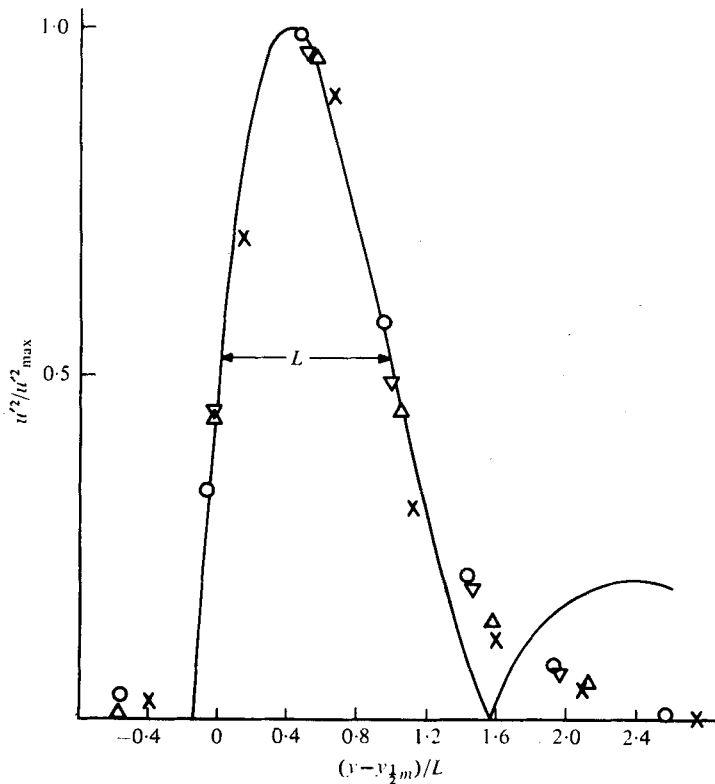
FIGURE 8. Distribution of u'^2/u'^2_{max} vs. $(y-y_{\frac{1}{2}m})/L$. $U_\infty = 35\,\text{ft/s}$, $x_{sp} = 1\,\text{ft}$. $\bigcirc$, $x_s = 3\,\text{ft}$, $z/x_s = 0.156$; $\triangle$, $x_s = 3\,\text{ft}$, $z/x_s = 0.128$; $\times$, $x_s = 3\,\text{ft}$, $z/x_s = 0.100$; ∇, $x_s = 2\,\text{ft}$, $z/x_s = 0.135$; ———, calculated distribution near branch I of neutral stability curve, $Re_* = 900$ (from Wazzan *et al.*).

The distribution of spectral peaks with distance from the surface is shown in figure 8. Initially, u'^2/u'_{max} was plotted *vs.* y/δ but it became apparent that δ is not the only characteristic length in the problem, in contradistinction to two-dimensional Tollmien–Schlichting waves. In fact, in order to collapse the data taken, at identical $Re_{\delta*}$ and y/δ but at different spanwise locations $(z/x_s) \geqslant 0.1$, onto a single curve, the abscissa had to be modified to include $y/\delta(z/x_s)^{\frac{1}{2}}$ because the boundary layer directly behind the spot is highly three-dimensional; i.e. it is thinnest in the plane of symmetry directly behind the trailing edge of the spot where the momentum thickness is equal to $\frac{1}{2}$ of that in the Blasius layer at a fixed Re_x (see Wygnanski *et al.* 1976, figure 19). The boundary layer thickens with increasing z until it attains its equilibrium value beyond the span of the spot. To overcome this difficulty u'^2/u'^2_{max} was plotted *vs.* $(y-y_{\frac{1}{2}m})/L$, where L represents the width of the u'^2 distribution (i.e. distance normal to the surface between two points at which $u'^2 = 0.5u'^2_{max}$) and $y_{\frac{1}{2}m}$ is the lesser value of y for which $u'^2 = 0.5\,u'^2_{max}$. Velocity perturbations for the Blasius profile at $Re_{\delta*} = 900$ (near branch I of the neutral stability diagram) are also included for comparison in the above mentioned co-ordinates. The effect of the spanwise fluctuations associated with the oblique waves was not taken into consideration. Wazzan, Okamura & Smith (1968) matched their minimal value of the eigenfunction solutions to the experimentally observed amplitudes of Schubauer & Skramstad (1948) in a similar manner
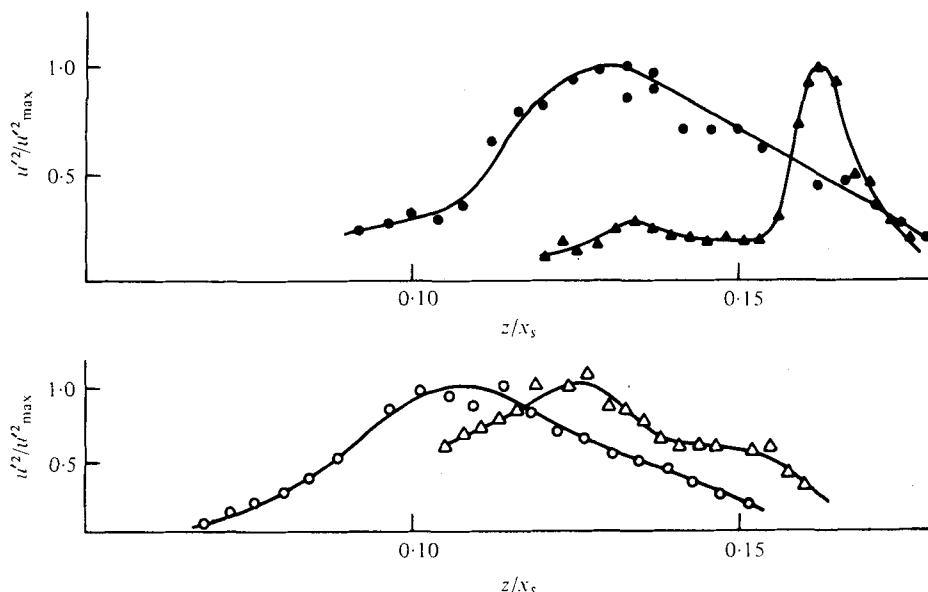
FIGURE 9. Distribution of u'^2/u'^2_{max} vs. z/x_s. $x_{sp} = 1$ ft. $\bigcirc$, $x_s = 2$ ft, $U_\infty = 35$ ft/s; $\triangle$, $x_s = 3$ ft, $U_\infty = 35$ ft/s; $\bullet$, $x_s = 2$ ft, $U_\infty = 65$ ft/s; $\blacktriangle$, $x_s = 3$ ft, $U_\infty = 65$ ft/s.

and the latter investigators equated the area under the theoretical and experimental curves.

Three-dimensional effects are not the only ones affecting the amplitude of the wave packet. The reader is reminded that the packet is located near a trailing edge of a large disturbance which alters the local velocity field. The choice of stability calculations based on the Blasius boundary layer does not consider the details of the actual unsteady flow in the space of interest.

4.3. *Nonlinear effects and onset of turbulence*

So far we have considered the wave packet as being quasi-two-dimensional although we recognized the finite length of the waves in the spanwise direction. The variation of the wave amplitude with z was estimated in the same manner as in the y direction. The centre of the Hanning window was aligned with the waves and thus was shifted in time to account for the inclination of the wave packet. The results are shown in figure 9.

Measurements were conducted at 2 and 3 feet downstream of the spark at $U_\infty = 35$ ft/s and $U_\infty = 65$ ft/s. At the lower freestream velocity the wave crests are fairly straight (figure 5) and their amplitude diminishes rapidly towards the centre of the spot and beyond its 'wing-tip'. Near the plane of symmetry, the local velocity profile is much more stable to small disturbances than the Blasius profile so the waves seem to terminate at the edge of the calming region. The location of maximum amplitude of the waves does not scale with the similarity length-scale of the spot (x_s).

If we assume that the maximum in the amplitude distribution is convected outwards as the wave packet proceeds downstream, then the angle between the convection velocity and the free stream is $10.4°$ ($\Delta z = 2.2$ in. for $\Delta x = 12$ in.). Since this is also the
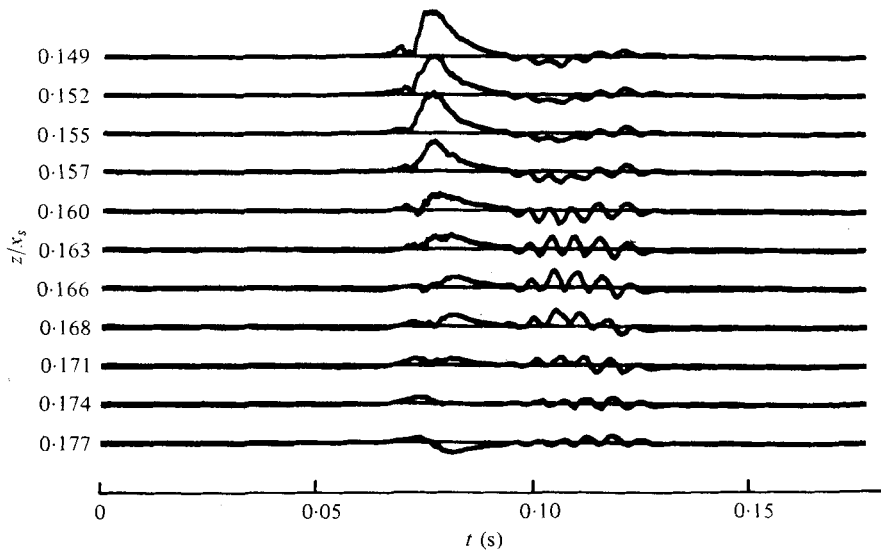
FIGURE 10. Ensemble average near tip of spot. $x_{sp} = 1$ ft, $x_s = 3$ ft, $y/x_s = 1 \cdot 1 \times 10^{-3}$, $U_\infty = 65$ ft/s.

angle at which the spot spreads in the z direction it would be surprising if it were a mere coincidence. It would appear from these simple geometrical considerations that the spot acts as a moving source for the generation and amplification of the waves.

Three feet downstream of the spark (at $U_\infty = 65$ ft/s) most of the wave activity is concentrated at the outer extremity of the spot ($z/x_s = 0 \cdot 17$). One could conclude from a simple observation of the spanwise distributions of u'^2 at $U_\infty = 35$ ft/s and 65 ft/s that any differences must stem from a Reynolds number effect; however, that is not the case. When the spark was moved to a location two feet downstream from the leading edge of the plate with all other parameters unchanged ($U_\infty = 65$ ft/s, $x_s = 2$ ft, $x_{sp} = 2$ ft), the spanwise distribution of u'^2 resembled the distribution at $x_s = 2$ ft, $U_\infty = 65$ ft/s and $x_{sp} = 1$ ft. Since all parameters based on the laminar boundary layer remained constant, a length dimension associated with the size of the spot must be of importance indicating that the spot may be the source of the wave activity with the boundary layer providing a receptive medium.

One does not have to resort to spectral analysis to observe the enhanced activity at the wing-tip of the spot. In figure 10 an ensemble-averaged distribuion of u shows that the large amplitudes in the wave packet are occurring mostly near the tip of the spot. The tip of the spot is marked by the appearance of a velocity defect which may be observed in the bottom trace of figure 10. Since the outer region of the spot in the direction normal to the surface has a characteristic velocity defect, the appearance of the defect in figure 10 implies that the average height of the spot is less than $0 \cdot 2 \delta$ at $z/x_s = 0 \cdot 177$.

The ensemble-average amplitude of the waves in the packet rapidly diminishes for $z/x_s < 0 \cdot 157$ and a long defect region modulating the entire packet appears behind the spot. The ensemble-averaged velocity behind the spot in that region at
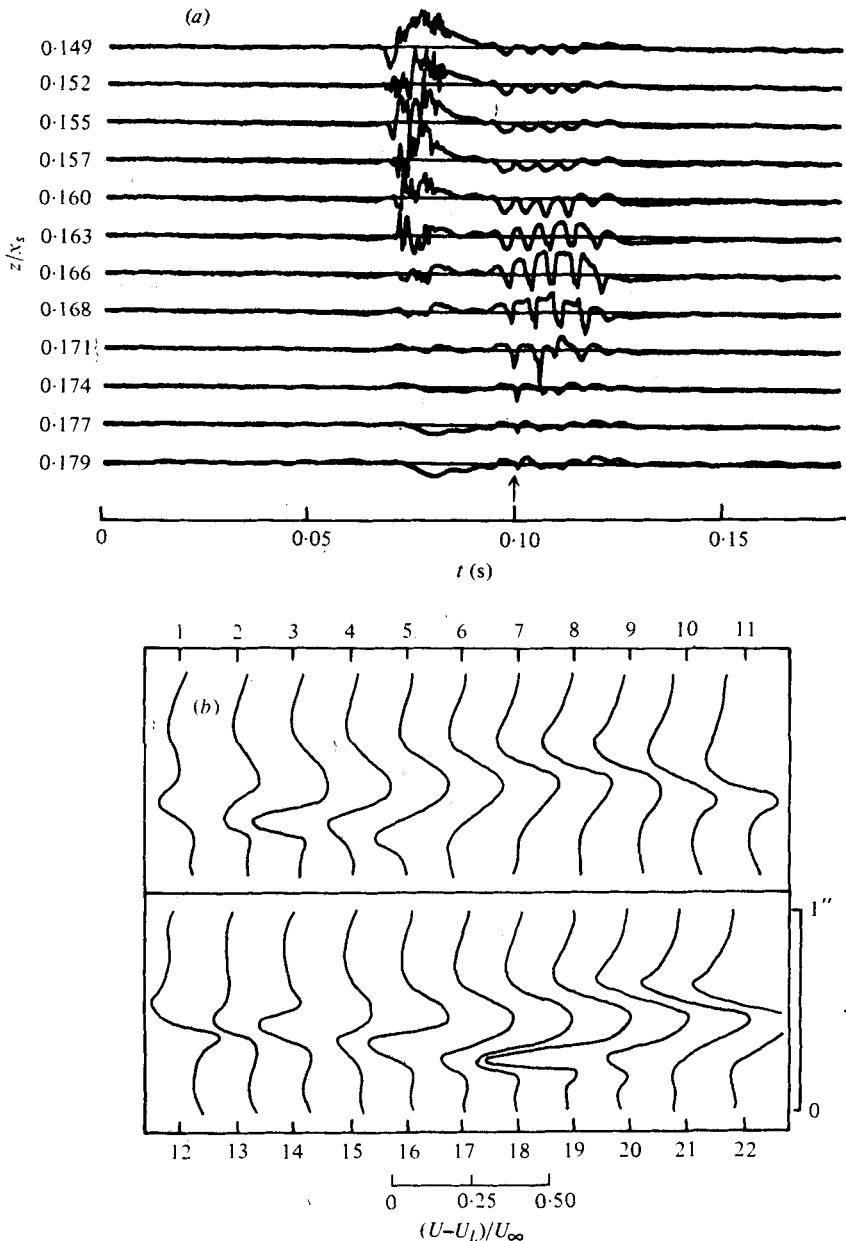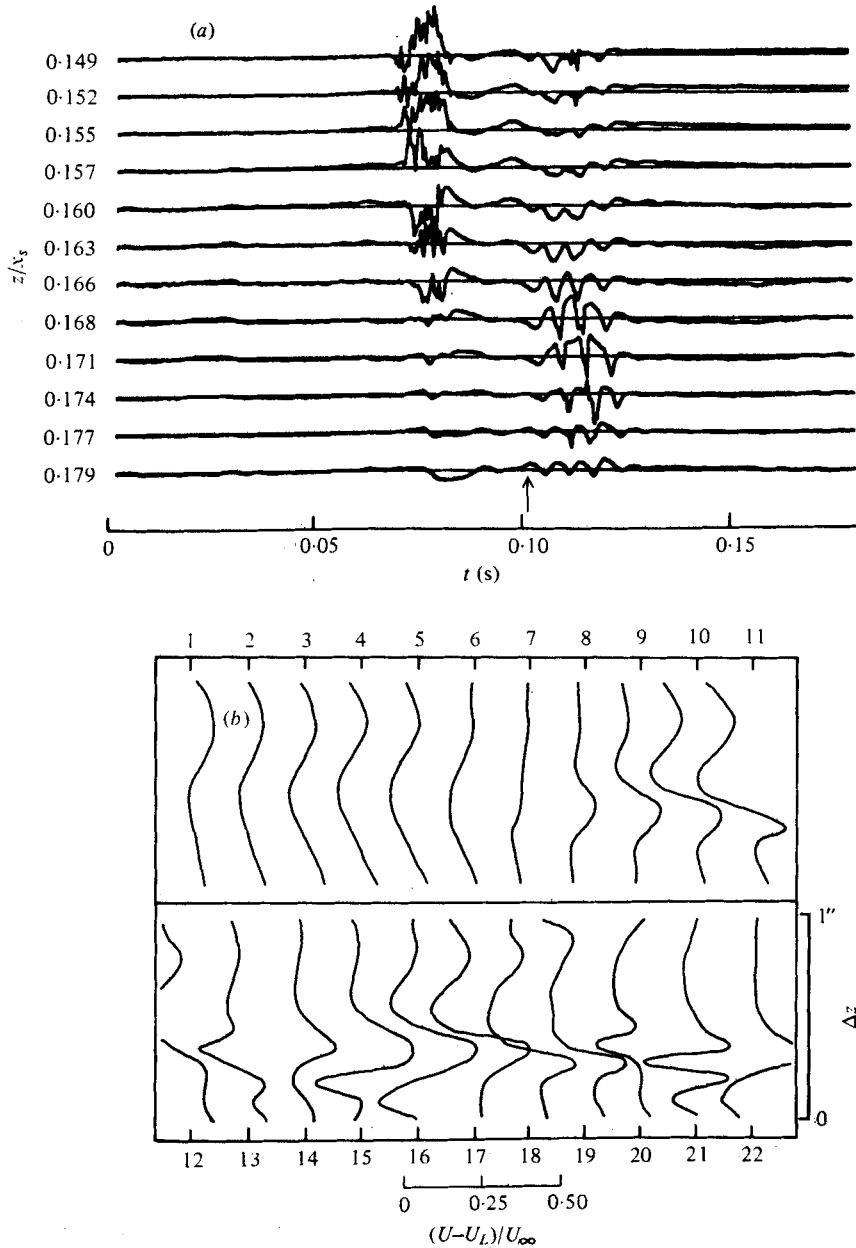
$$y/x_s = 1 \cdot 1 \times 10^{-3}$$

FIGURE 11. Example of breakdown in the z direction. $x_{sp} = 1$ ft, $x_s = 3$ ft, $y/x_s = 1.1 \times 10^{-3}$, $U_\infty = 65$ ft/s. (a) The arrow indicates the location of the first profile in (b). (b) Velocity profiles vs. z at time intervals of $\Delta t = 0.0008$ s.

drops below the velocity existing in the laminar boundary layer (Blasius profile). It may be inferred that the waves break around this spanwise location.

The breakdown process may be observed by examining individual realizations which are shown in figures 11 and 12. The first part of each figure gives a temporal record of u as obtained from the 12 hot wires in the z rake and the second part gives instantaneous

FIGURE 12. Example of breakdown in the z direction. $x_{sp} = 1\,\mathrm{ft}$, $x_s = 3\,\mathrm{ft}$, $y/x_s = 1.1 \times 10^{-3}$, $U_\infty = 65\,\mathrm{ft/s}$. (a) The arrow indicates the location of the first profile in (b). (b) Velocity profiles *vs.* z at time intervals of $\Delta t = 0.0016\,\mathrm{s}$.

velocity profiles in the z direction. All measurements were taken at a constant distance from the surface. In figure 11 (a) the breakdown region is bounded by $0.16 < z/x_s < 0.21$ with the regular waves being observed for $0.1 < z/x_s < 0.15$.

In the region $0.15 < z/x_s < 0.16$ a low frequency oscillation appears behind the spot which resembles the low frequency oscillation at the very tip of the original spot.
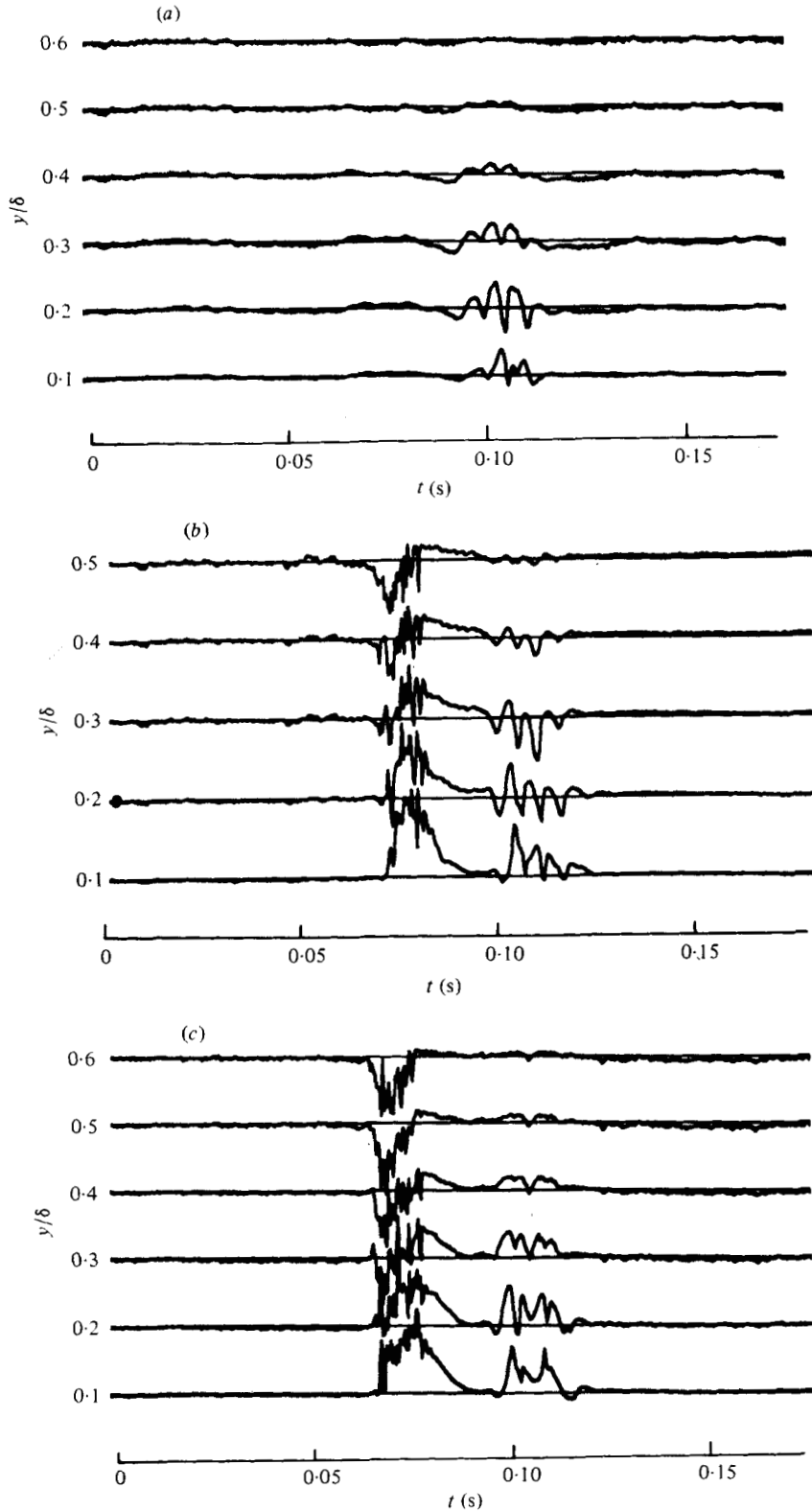
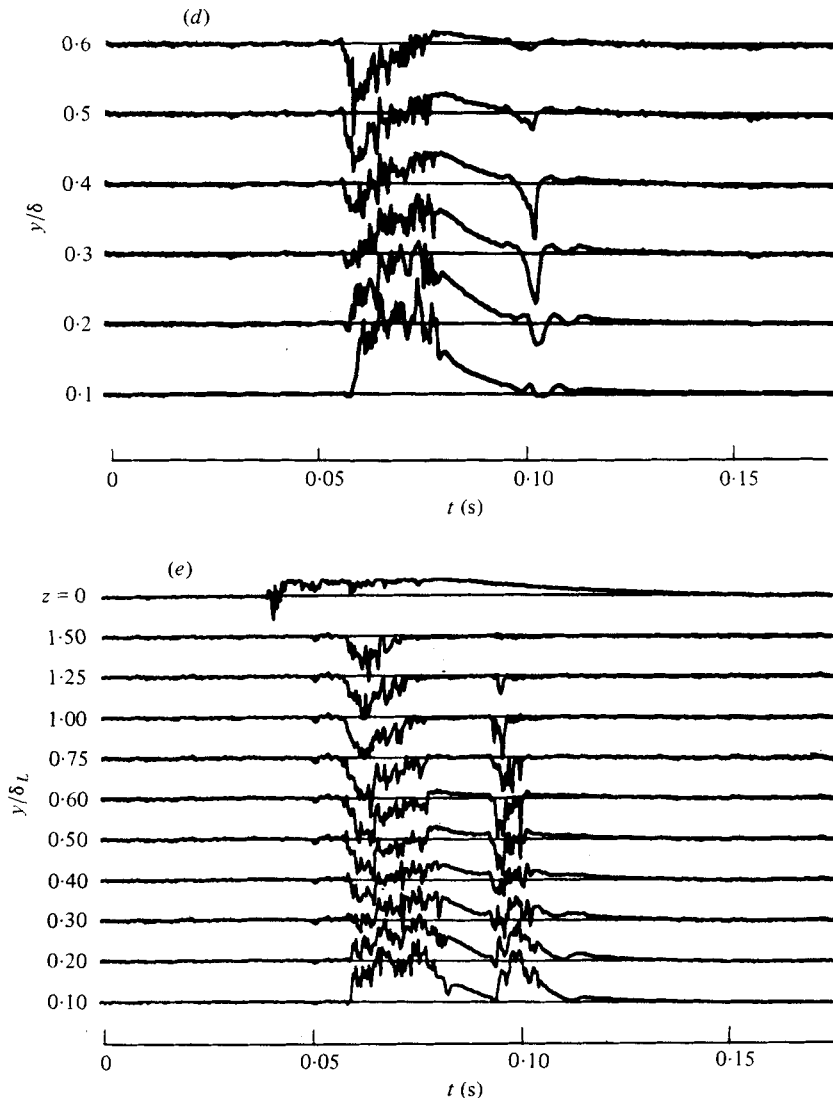FIGURE 13 (*a–c*). For legend see facing page.

FIGURE 13. Examples of breakdown in the y direction. $x_{sp} = 1\,\text{ft}$, $x_s = 3\,\text{ft}$, $U_\infty = 65\,\text{ft/s}$. (a) $z/x_s = 0.171$; (b) $z/x_s = 0.143$; (c) $z/x_s = 0.143$; (d) $z/x_s = 0.115$; (e) $z/x_s = 0.115$.

We thus may be seeing the creation of a new spot upstream of the original one. The amplitude of the 'spikes' in the u component of the velocity at the onset of breakdown is extremely large. The spike recorded by the wire which is located at $z/x_s = 0.171$ indicates the possibility that the flow is brought close to stagnation. Although one cannot rely on the response of the hot wire in this particular instance, the average amplitude of the spikes at breakdown is on the order of $0.4U_\infty$. This is very consistent with the observations of Klebanoff *et al.* (1962). Two traces at $z/x_s = 0.171$ and at $z/x_s = 0.174$ (figure 12a) indicate that at one point in time when a spike directed towards a lower velocity occurs at $z/x_s = 0.171$ an opposite velocity perturbation occurs $0.1\,\text{in.}$ away. This defines a width of a very intense shear layer which exists

momentarily between the two wires. Instantaneous velocity perturbations in the z direction enable us to have a glimpse into the breakdown process. Twenty-two profiles are shown in each figure; however, the time lapse between consecutive profiles in figure 12(b) is double that of figure 11(b). (Δt between profiles = 0·0016 s in figure 12b). The velocity scale is shown at the bottom of the figures with positive perturbation of velocity to the right of the tick marks. Profiles 1–5 in figure 12(b) have a typical S shape which results from the inclination of the wave front from the plane of symmetry. Similar velocity profiles are observed at lower velocities in the absence of breakdown. A phase shift in the wave pattern is observed in profiles 6 and 7 followed by the creation of a strong shear layer with vorticity normal to the surface of the plate. Extremely concentrated shear layers appear in profile 19 of figure 11(b) and in profile 21 in figure 12(b). The width of such shear layers is at most 0·1 in. (i.e. the spatial resolution of the measurement) while the velocity jump across it reaches 35 % U_∞. Thus, at breakdown $\partial u/\partial z$ can become comparable to $\partial u/\partial y$, which is considered to be the dominant factor in boundary layer stability. Komoda (1967) observed that whenever there is a considerable spanwise variation in the boundary-layer thickness, as is the case near the 'wing-tip' of the turbulent spot, breakdown is preceded by a concentration of vorticity in a thin vertical layer, thus the appearance of such shear layers in the present experiment should not be surprising. Typically those shear layers are very long in comparison to their lateral dimension and we conclude, albeit from a small sample of observations, that the dominant aspect ratio of these layers is:

$$0.025 \leqslant z/tU_\infty \leqslant 0.05.$$

These numbers are in agreement with pictures visualizing sublayer streaks in a turbulent spot (Cantwell *et al.* 1977).

Instantaneous observations in the y, t plane were made with the 10-wire y probes at various spanwise and streamwise locations. The most interesting observations are those showing the breakdown of the wave packet and the generation of a new spot. Results from five or six hot wires located at $x_s = 3$ ft and $y/\delta = 0·1$ are shown in figure 13. Near the tip of the spot ($z/x_s = 0·171$) breakdown is most often seen near the surface; the customary 'spike' which usually occurs at the outer region of the layer was not observed (figure 13a). The large amplitude fluctuations at $y/\delta = 0·1$ (figure 13b, c) all show an increase in velocity suggesting that the wall shear-stress increases at the very early stages of transition. Although the events recorded in figure 13(b, c) appeared at identical positions ($z/x_s = 0·143$), figure 13(c) shows the onset of turbulence and the generation of a new spot slightly more clearly. The u trace at $y/\delta = 0·1$ shows how a wave packet containing 4 waves breaks down generating two spikes; the first one will most probably mark the leading edge of a new spot, and the second its trailing edge. Closer to the plane of symmetry single 'spikes' are more often observed (figure 13d), but they occur closer to the surface than could be expected from measurements of Klebanoff *et al.* (1962). In this case most of the 'spikes' occur at $0·3 < y/\delta < 0·4$ rather than $y/\delta = 0·7$ observed in the experiments with vibrating ribbons (Kovasznay, Komoda & Vasudeva 1962; and Klebanoff *et al.* 1962). A new spot trailing the original one is observed in figure 13(e). The observation shown is still at $U_\infty = 65$ ft/s and $z/x_s = 0·115$ where the single spike (figure 13d) was also seen. Thus the new turbulence generated is not very well controlled in the present experi-
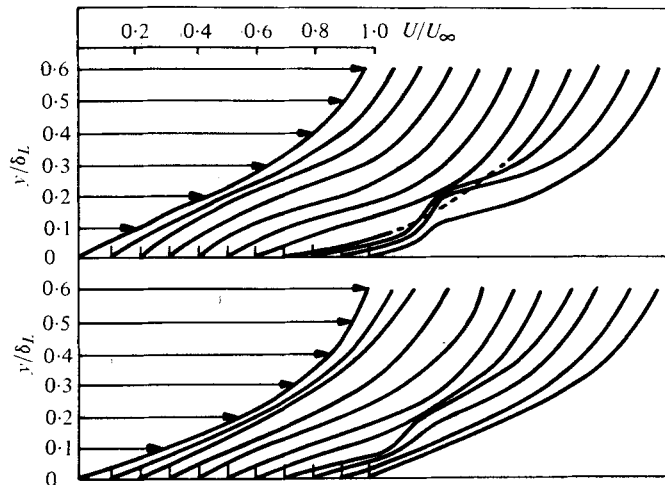
FIGURE 14. Instantaneous velocity profiles at breakdown from figure 13(c). $\Delta t = 0.0008$ s between profiles.

mental set up. The uppermost trace in figure 13(e) shows a simultaneous record from a second probe which was located on the plane of symmetry of the spot. This wire does not show any signs of secondary breakdown. Thus we conclude that new spots are generated outside the calmed region at $z/x_s > 0.1$.

The data from figure 13(c) was replotted to show instantaneous velocity profiles in the plane vertical to the surface at $z/x_s = 0.143$. Some of these profiles are similar to the profile measured by Klebanoff *et al.* (1962) at breakdown (station D in their paper) and behind a hemispherical roughness element. The profiles in figures 11(b), 12(b) and 14 indicate that the generation of high frequency oscillations in the boundary layer can be related to the stability of inflexional flows like the mixing layer. The flow is, however, highly three-dimensional and even for an observer moving with the wave crest it may not be a steady one.

By removing the high-frequency content from the signals (i.e. using a digital low-pass filter) oscillations in the Tollmien–Schlichting frequency range seem to reappear inside the spot even near the plane of symmetry. The oscillations are no longer coherent in the spanwise direction and they cannot be deduced in the same way as the waves near the tip of the spot were, but they seem to persist inside the turbulent region. A time scale corresponding to the appropriate Tollmien–Schlichting frequency is sketched in figure 15(b, d) for comparison. The unfiltered streamwise velocities are not highly correlated in the spanwise direction, yet there seems to be a fairly high degree of coherence in the direction normal to the plate, figure 16. Chen (1972) associates the events having a high degree of correlation in the normal direction, with the occurrence of 'bursts' in a turbulent boundary layer. Bursts, therefore, most probably exist in an isolated spot.
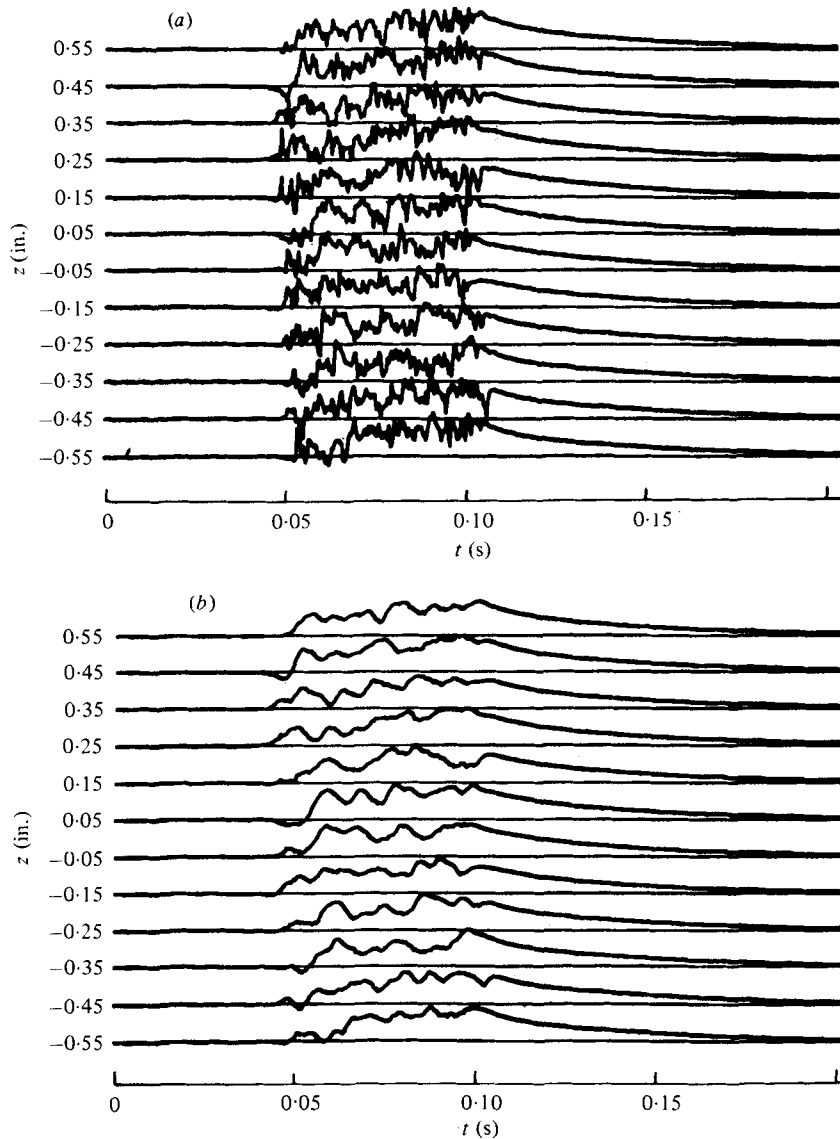
FIGURE 15 (*a, b*). For legend see facing page.

5. Conclusions

The oblique wave packet which was found to trail the transitional spot is an important element of the transition process. The original oscillograms of Schubauer & Skramstad (1948) showing natural oscillations in the boundary layer of a flat plate indicate that the waves appear in packets and not in a continuous wave train, such as those later generated by a vibrating ribbon. According to the linear stability theory the waves which we have observed are the most amplified ones. The weak packet generated by Gaster & Grant (1975) bears certain similarities to the packet observed here.

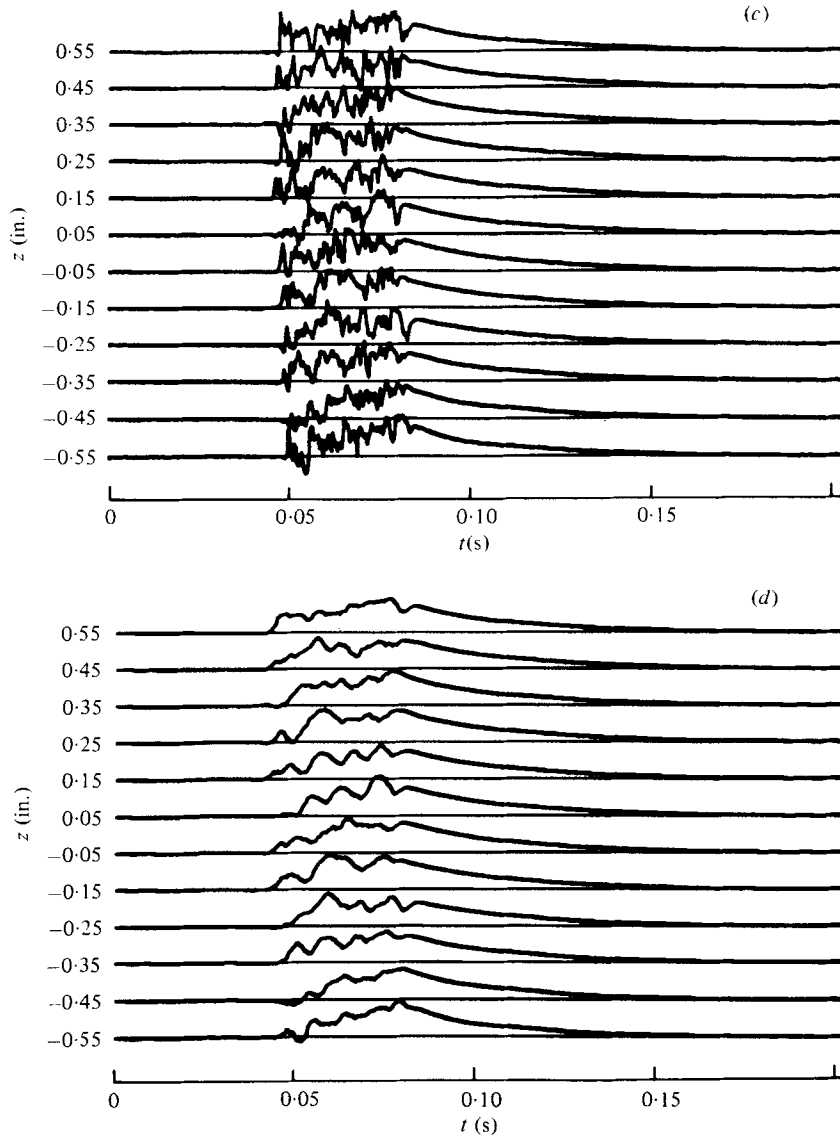(1) The maximum spreading angle of their packet in the spanwise direction is

FIGURE 15. Waves inside spot. $x_{\text{sp}} = 1\,\text{ft}$, $x_s = 3\,\text{ft}$, $y/x_s = 1\cdot3 \times 10^{-3}$, $z \sim$ centreline of spot, $U_\infty = 35\,\text{ft/s}$. (*a*) Unfiltered. (*b*) Low pass filtered with $f_c = 150\,\text{Hz}$. (*c*) $x_s = 2\,\text{ft}$, $y/x_s = 1\cdot7 \times 10^{-3}$; unfiltered. (*d*) Low pass filtered with $f_c = 150\,\text{Hz}$.

$10\cdot6°$. In our case the peak of the wave energy spreads at $10\cdot4°$ and this is also the maximum spreading angle of the spot itself. The calculated spanwise component of the group velocity yields an angle of the same magnitude.

(2) The envelope of their packet is convected downstream with a velocity of $0\cdot44U_\infty$. The streamwise component of the packet's group velocity is approximately $0\cdot42U_\infty$ in the present case.

Although a coherent wave packet is only observed behind the spot outside the calmed region, waves of the appropriate frequency are apparent inside the turbulent spot itself. It is thus felt that the shape of the spot, its rate of growth and its spreading
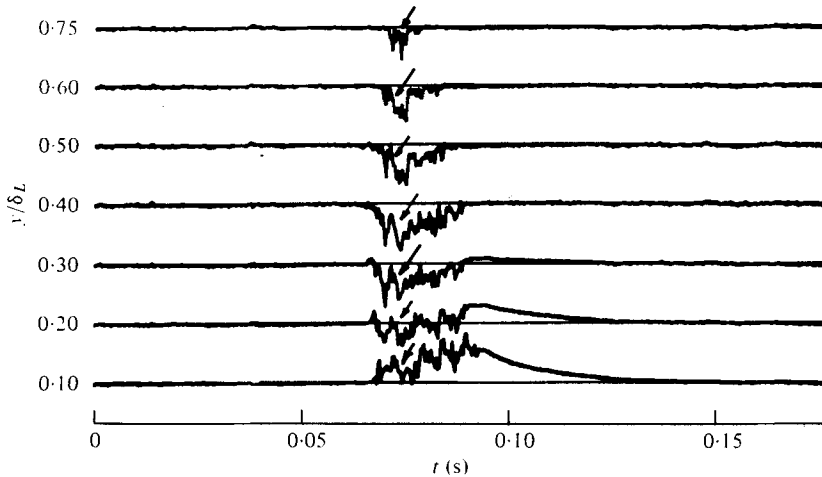
FIGURE 16. Coherence in the y direction inside the spot.
$x_{,p} = 2\,\text{ft}, x_s = 2\,\text{ft}, U_\infty = 65\,\text{ft/s}.$

angle are related to the wave packet. At high Reynolds numbers (based on some characteristic spot dimension) the spot generates new spots setting a chain reaction by which turbulence spreads rapidly covering the entire flow field. The wave packet breaks down by generating strong shear layers in both the spanwise and normal directions and inflexional profiles are observed in both directions with $\partial u/\partial z$ being comparable in magnitude to $\partial u/\partial y$. The intense vertical shear layers have a characteristic dimension which is similar to the dimension of the wall streaks in a fully turbulent boundary layer. Since these shear layers are not perfectly aligned with the direction of the free stream, observations at a single point may indicate a deceleration of the flow which in turn may be interpreted as a burst. The coherence of the large structures in the y direction is generally better than the coherence in the spanwise direction.

Appendix
Squire's transformation

Squire (1933) showed that the eigenvalue problem of an oblique (to the mean flow) three-dimensional wave can be reduced to that of a simple (wavenumber parallel to the mean flow) two-dimensional wave after certain substitutions are made. Although this is a well-known transformation there seem to be differences in interpretation between the present work and the literature (Betchov & Criminale 1967; Drazin & Howard 1966; Gaster 1968). The purpose of the following exercise is to clarify these differences.

Quantities with subscript 3 refer to the oblique wave and with subscript 2 to the simple one. Following Squire's general approach, a mean flow, parallel to a flat plate, is considered for an oblique wave with

$$U_3 = U_3(y), \quad V_3 = 0, \quad W_3 = 0 \tag{1}$$

in the directions x, y, z respectively, where y is the co-ordinate perpendicular to the plate. The disturbances are assumed to be periodic of the form

$$\left.\begin{array}{l} (u, v, w) = (u(y), v(y), w(y)) \exp\left[i(\alpha_3 x + \beta_3 z - \omega_3 t)\right], \\ p = p(y) \exp\left[i(\alpha_3 x + \beta_3 z - \omega_3 t)\right], \end{array}\right\} \tag{2}$$

where the u, v, w and p are the velocity and pressure perturbations respectively. α_3 and β_3 are the wave numbers in the x and z directions and ω_3 is the frequency. If one considers the temporal problem then α_3 and β_3 are real and ω_3 is in general complex, ω_3 being real representing a neutral wave. Substituting relations (1) and (2) into the equations of motion, linearizing and regrouping, one obtains, after some algebra,

$$\left\{\frac{i\nu_3}{\alpha_3}\left[\frac{\partial^2}{\partial y^2} - (\alpha_3^2 + \beta_3^2)\right]^2 + \left(U_3 - \frac{\omega_3}{\alpha_3}\right)\left[\frac{\partial^2}{\partial y^2} - (\alpha_3^2 + \beta_3^2)\right] - \frac{\partial^2 U_3}{\partial y^2}\right\} v_3 = 0 \tag{3}$$

with boundary conditions

$$v_3 = 0 \quad \text{at} \quad y = 0, \quad y = +\infty; \quad \frac{\partial v_3}{\partial y} = 0 \quad \text{at} \quad y = 0, \quad y = +\infty.$$

Following the same procedure for a simple two-dimensional wave yields

$$\left\{\frac{i\nu_2}{\alpha_2}\left(\frac{\partial^2}{\partial y^2} - \alpha_2^2\right) + \left(U_2 - \frac{\omega_2}{\alpha_2}\right)\left(\frac{\partial^2}{\partial y^2} - \alpha_2^2\right) - \frac{\partial^2 U_2}{\partial y^2}\right\} v_2 = 0. \tag{4}$$

Effectively (4) can be obtained from (3) by setting $\beta_3 = 0$ and changing the subscripts from 3 to 2. At this point it should be emphasized that Squire's transformation is the result of a simple mathematical substitution and has, as stated, no physical significance. It stems from the realization that the eigenvalue problem posed by (3) is *mathematically* identical to that posed by (4) if and only if

$$i\nu_3/\alpha_3 = i\nu_2/\alpha_2, \quad \alpha_2^2 = \alpha_3^2 + \beta_3^2, \quad \omega_3/\alpha_3 = \omega_2/\alpha_2. \tag{5}$$

The only wave descriptor preserved in this equivalence is the magnitude of the wave-number vector, the mean flow being the same for both cases.

The literature cited earlier is in agreement with (5); however, it states that the phase speed is the same for both waves. What is the same is the quantity ω_i/α_i since

$$c_2 = \omega_2/\alpha_2, \quad c_3 = \omega_3/(\alpha_3^2 + \beta_3^2)^{\frac{1}{2}} \neq c_2.$$

ω_3/α_3 is the crest speed in the streamwise direction and since it is a convenient experimental quantity it may be useful to define it as the crest speed c_{cr}, in the x direction in this case:

$$c_{\mathrm{cr}} \equiv \omega_3/\alpha_3 = c_3/\cos\psi,$$

where ψ is the angle between the wavenumber vector and the streamwise direction.

In order to 'place' an oblique wave on the usual two-dimensional stability diagram the actual viscosity ν should be replaced by $\nu/\cos\psi$ and the actual frequency f by $f/\cos\psi$. The actual non-dimensional wavenumber $(\alpha_3^2 + \beta_3^2)^{\frac{1}{2}}$ or α_2 is not affected. The actual phase speed of the oblique wave, i.e. in the direction ψ, is $c_2\cos\psi$.

REFERENCES

BETCHOV, R. & CRIMINALE, W. O. 1967 *Stability of Parallel Flows.* New York: Academic Press.

BLACKWELDER, R. F. & KAPLAN, F. E. 1976 *J. Fluid Mech.* **76**, 89.

CANTWELL, B., COLES, D. & DIMOTAKIS, P. 1977 *California Inst. Tech., Dept. Aeronaut. Interim Rep.* ENG-7680150.

CHEN, P. C. 1972 Ph.D. Thesis, University of South California.

COLES, D. & BARKER, S. J. 1975 *Turbulent Mixing in Nonreactive and Reactive Flows,* p. 285. Plenum Press.

DRAZIN, P. G. & HOWARD, L. N. 1966 *Advances in Applied Mechanics.* New York: Academic Press.

ELDER, J. 1960 *J. Fluid Mech.* **9**, 235.

EMMONS, H. W. 1951 *J. Aero. Sci.* **18**, 490.

GASTER, M. 1968 *J. Fluid Mech.* **32**, 173.

GASTER, M. & GRANT, I. 1975 *Proc. Roy. Soc.* A **347**, 253.

KAPLAN, R. E. 1964 *M.I.T. Rep.* ASRL TR-116-1.

KLEBANOFF, P. S., TIDSTROM, K. D. & SARGENT, L. M. 1962 *J. Fluid Mech.* **12**, 1.

KOMODA, H. 1967 *Phys. Fluids Suppl.* **10**, S 87.

KOMODA, H. 1974 Private communication (I.W.)

KOVASZNAY, L. S. G., KIBENS, V. & BLACKWELDER, R. F. 1970 *J. Fluid Mech.* **41**, 283.

KOVASZNAY, L. S. G., KOMODA, H. & VASUDEVA, B. R. 1962 *Proc. Heat Transfer Fluid Mech. Inst.,* Stanford Univ. Press.

LANDAHL, M. T. & KAPLAN, R. E. 1965 *Agardograph* 97, part I, p. 363. Paris.

MOCHIZUKI, M. 1961 *J. Phys. Soc. Japan,* **16**, 995.

OSTER, D., WYGNANSKI, I. & FIEDLER, H. 1976 In *Turbulence in Internal Flows* (ed. S. N. B. Murthy), p. 67. Hemisphere Press.

SCHUBAUER, G. B. & KLEBANOFF, P. S. 1956 *N.A.C.A. Rep.* no. 1289.

SCHUBAUER, G. B. & SKRAMSTAD, H. K. 1947 *N.A.C.A. Tech. Rep.* no. 909.

SQUIRE, H. B. 1933 *Proc. Roy. Soc.* A **142**, 621.

WAZZAN, A. R., OKAMURA, T. T. & SMITH, A. M. O. 1968 DAC-67086, Sept. 1, 1968. McDonnell Douglas Corp.

WYGNANSKI, I., SOKOLOV, M. & FRIEDMAN, D. 1975 *J. Fluid Mech.* **69**, 283.

WYGNANSKI, I., SOKOLOV, M. & FRIEDMAN, D. 1976 *J. Fluid Mech.* **78**, 785.

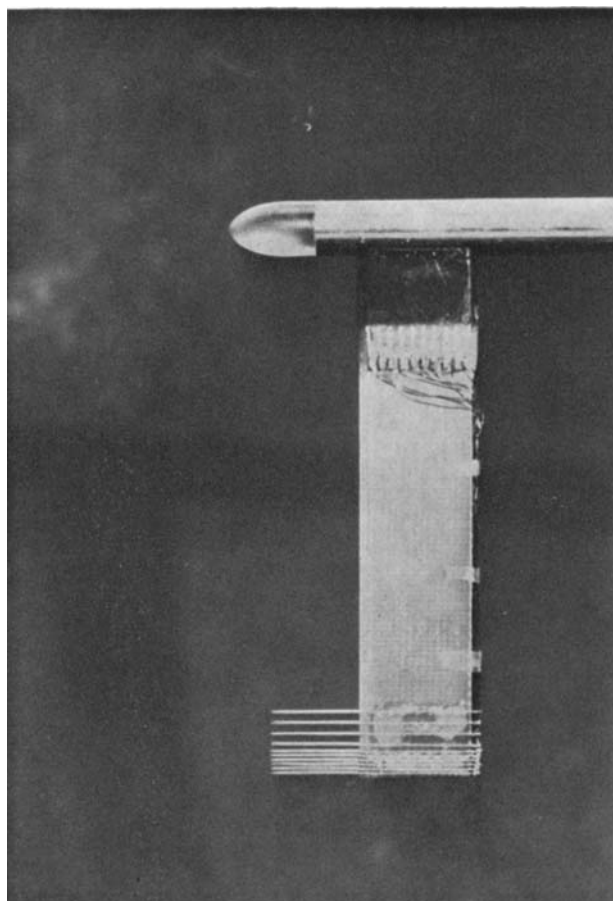ZILBERMAN, M., WYGNANSKI, I. & KAPLAN, R. E. 1976 *Phys. Fluids Suppl.* **20**, S 258.
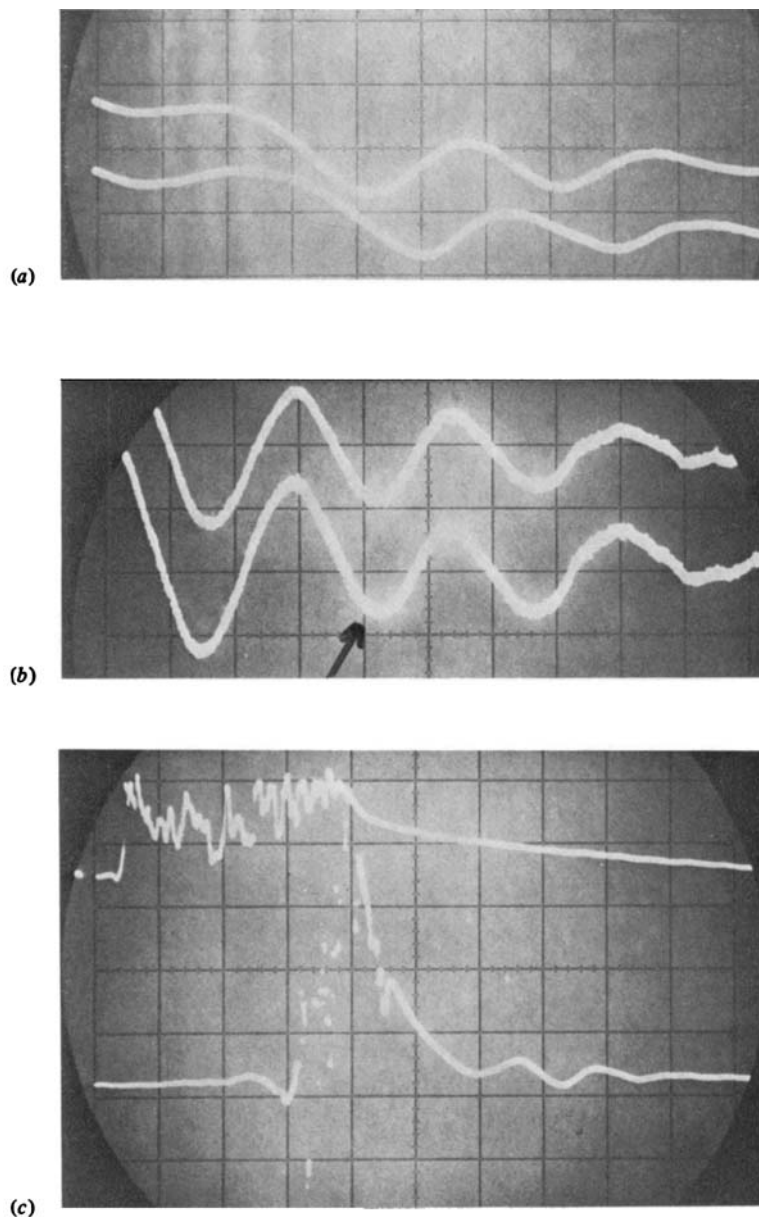
FIGURE 1. Small y rake probe and holder.

FIGURE 3. Gross characteristics of wave packet. $x_{sp} = 1\,\text{ft}$, $x_s = 2\,\text{ft}$, $U_\infty = 35\,\text{ft/s}$. (a) Crest speed: $\Delta x = 0.75\,\text{in.}$, $\Delta z = \Delta y = 0\,\text{in.} \to c_{cr} = 0.4U_\infty$. (b) Inclination of wave packet: $\Delta x = 0.49\,\text{in.}$, $\Delta z = 0.45\,\text{in.} \to \psi = 47°$. (c) Location of wave packet: upper trace in plane of symmetry; lower trace at $z/x_s = 0.21$.

WYGNANSKI, HARITONIDIS AND KAPLAN